ANNALS OF GEOPHYSICS, 61, 4, SE444, 2018, doi: 10.4401/ag-7604

“ITALIAN RADON MONITORING NETWORK (IRON): A PERMANENT NETWORK FOR NEAR REAL-TIME MONITORING OF SOIL RADON EMISSION IN ITALY”

Valentina Cannelli[1,*], Antonio Piersanti[1], Gianfranco Galli[1], Daniele Melini[1]

[(1)] Istituto Nazionale di Geofisica e Vulcanologia, Roma, Italy

Article history
Receveid **December 12, 2017**; accepted **May 21, 2018.**
Subject classification:
Radon; Near real-time monitoring, Permanent dense network; Time series analysis; Measurement methodology.

ABSTRACT

We introduce the Italian Radon mOnitoring Network (IRON): a new nationwide permanent network for near real-time measurements of soil radon emissions in Italy. Deployed over the last 9 years, presently IRON consists of 26 stations mainly concentrated in the Central-Southern Apennines, but marginally covering the whole Italian peninsula. At present, most IRON stations have recorded radon concentration time-series for more than 4-5 years. With a standard sampling interval of about two hours, the whole IRON dataset consists of nearly 440,000 single radon concentration measurements. Here we present the network in terms of sites, installations types and collected time series. The amount of data, together with the systematic methods of measurements, allowed us to evaluate some significant aspects related both to the measurement methodology and to the complex dynamics of soil radon emanations. Two case studies show, respectively, how different observational setups impact on the features of the recorded signal, and how observed fluctuations in radon concentration may be ascribed to geophysical processes taking place at depth in the crust. We discuss the potential suitability of IRON, in order to study the relation between radon variability and the preparation processes of strong earthquakes.

1. INTRODUCTION

In multidisciplinary Earth science, radon is currently considered an efficient marker of the dynamic phenomena taking place in the Earth's crust and involving fluid migration and pressure transients. Due to its short half-life (3.82 days), its mobility in the ground by diffusion is limited, and carrier fluids (such as CO_2, CH_2 or N_2) are likely to play a major role in its dynamics. Evidence gathered in recent years indicates that, in specific seismotectonic settings, fluid transport could play an important role in stress changes associated with the preparatory stages of an earthquake [Miller et al., 2004; Stefansson, 2011; Lewicki et al., 2014; Jaishi et al., 2014; Shelly et al., 2015; Singh et al., 2016]. Recently, laboratory experiments confirmed evidence of the relation between the state of stress of a rock sample and variations in its radon emanation properties, allowing to assess radon variability under controlled conditions, i.e. without contamination by external factors such as meteorological effects [Tuccimei et al., 2010; Mollo et al., 2011; Cannelli et al., 2016]. These results ignited new interest in searching associations between variations in soil radon emissions and processes taking place on major tectonic faults, resulting from mechanical cracks in the rocks or slow crack growth determined by local strain of the media. A full review on recent literature about radon as earthquake precursor comparing methods, statistical analyses and results can be found in Woith, 2015.

From a technological point of view, radioactive detectors (as those used in the measurement of radon concentration) actually represent the most sensitive instruments, because sensitivity and efficiency in detecting and measuring ionizing radiation are much higher than any other non-radioactive element-detect-

ing instrument [Semkow et al., 1994; Abbady et al., 2004]. Moreover, their implementation and installation requirements make them also particularly competitive in terms of operating costs [Piersanti et al., 2015]. The cost factor becomes particularly important when the goal is the implementation of dense, permanent networks, covering wide regions. Such observation networks for the measurement of radon emissions are presently rare [Hauksson and Goddard, 1981; Inan and Seyis, 2010].

Here we describe the IRON network in terms of the observational setup employed in stations and discuss the basic features of the recorded time series. We illustrate two important case studies that demonstrate the scientific potential of the monitoring capabilities offered by IRON. Recent results [Stefansson, 2011; Piersanti et al., 2015; Cannelli et al., 2016; Piersanti et al., 2016; Singh et al., 2017] convinced us that progresses in the use of radon for the study of physical processes taking place at depth in the crust, as well as major earthquake preparation processes, rely on high-resolution and continuous long-term measurements granted by a permanent network.

2 THE IRON NETWORK

IRON is a monitoring network recording radon emission in terms of near real-time continuous concentration (Bq/m^3) that covers a wide regional-scale zone in Italy (Figure 1). Its implementation began in 2009, with the aim of designing and developing a network of permanent stations for the continuous monitoring of radon concentration in seismically active areas, in order to explore the possibility of a physical link between seismogenic processes and temporal variability in radon emissions [Piersanti et al., 2015; Cannelli et al., 2016; Piersanti et al., 2016]. Most stations are equipped with a proprietary detector based on a Lucas cell with a continuous data acquisition front-end, configured with an acquisition window of about 2 hours (115 minutes of data acquisition followed by a 5 minutes standby time). All stations are equipped with a local temperature sensor, while newer ones include also atmospheric pressure and humidity probes. Details of radon monitoring sites are reported in Table 1. Since 2009, 26 stations have been set up (see Figure 2), mainly concentrated in the Central-Southern Apennines, following the highest-ranked zones in the Seismic Hazard Map of Italy (MPS04, Mappa di Pericolosità Sismica 04: Seismic Hazard Map, in English - Ordinanza del Presidente del Consiglio dei Ministri, OPCM, 2006). Additional stations provide marginal coverage of

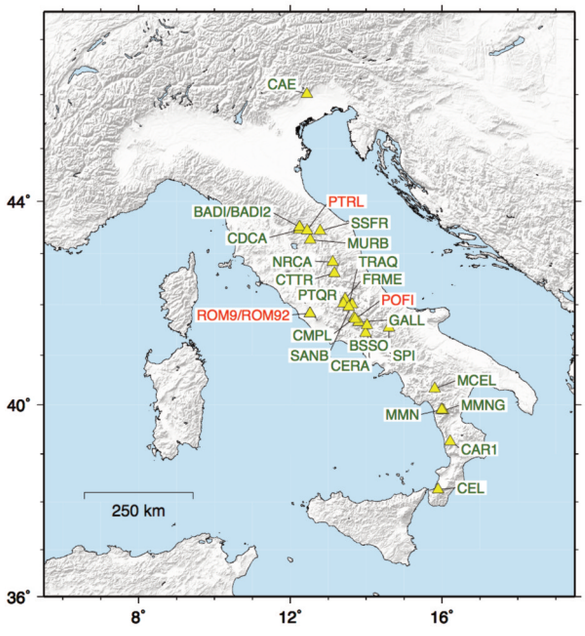

FIGURE 1. Layout of IRON network, as of November 2017. Green and red labels correspond to operating and discontinued stations, respectively.

the whole Italian peninsula. Six out of the 26 stations (PTRL - no longer operational, MURB, SSFR, CDCA, BADI, BADI2) have been installed in the framework of the multidisciplinary grant "The Alto tiBerina near fault ObservatOry" TABOO (http://taboo.rm.ingv.it, Chiaraluce et al. 2014), a research infrastructure included in the European Plate Observing System EPOS (https://www.epos-ip.org) framework and devoted to study earthquake preparatory processes. As reported in Table 1, several IRON stations are co-located with seismic and/or geodetic stations of major Italian seismic monitoring networks (INSN-INGV, Italian National Seismic Network and OGS, Istituto Nazionale di Oceanografia e di Geofisica Sperimentale).

The main rationale behind the IRON network is to in-

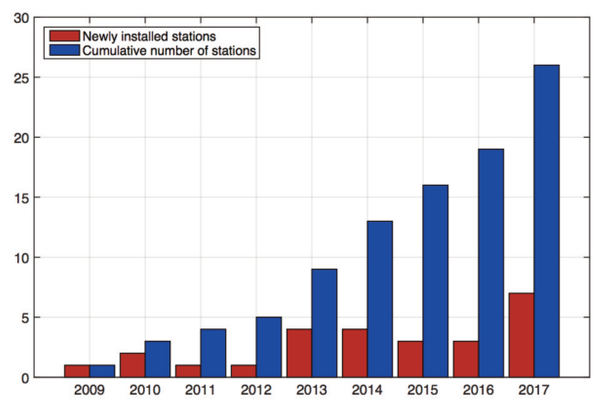

FIGURE 2. Evolution of the IRON network since 2009.

No	Code	Lat	Lon	Elev (m)	Parameter	Location	Installation type	Network
1	BADI	43.509	12.244	430	CRn, iT	Badiali (PG, Umbria)	Shelter	INGV-INSN
2	BADI2	43.509	12.244	430	CRn, iT	Badiali (PG, Umbria)	Soil	INGV-INSN
3	CAE	46.009	12.437	870	CRn, iT	Caneva (PN, Friuli Venezia-Giulia)	Borehole	OGS
4	CDCA	43.458	12.233	50	CRn, iT	Città di Castello (PG, Umbria)	Shelter	INGV-INSN
5	CMPL	41.737	13.678	650	CRn, iT	Campoli Appennino (FR, Lazio)	Indoor	IRON
6	CTTR	42.617	13.159	960	CRn, iT	Cittareale (RI, Lazio)	Indoor	IRON
7	FRME	42.111	13.442	1012	CRn, iT	Forme (AQ, Abruzzo)	Indoor	IRON
8	GALL	41.674	13.817	452	CRn, iT	Gallinaro (FR, Lazio)	Indoor	IRON
9	MCEL	40.324	15.801	960	CRn, iT, iP	Monticello (PZ, Basilicata)	Soil	INGV-INSN
10	MMN	39.899	15.990	921	CRn, iT	Mormanno Faro (CS, Calabria)	Indoor	INGV-INSN
11	MMNG	39.885	16.025	858	CRn, iT	Mormanno Ghiro (CS, Calabria)	Indoor	IRON
12	MURB	43.263	12.524	854	CRn, iT	Monte Urbino (PG, Umbria)	Borehole	INGV-INSN
13	NRCA	42.833	13.114	927	CRn, iT	Piè La Rocca (PG, Umbria)	Shelter	INGV-INSN
14	POFI	41.717	13.712	878	CRn, iT	Posta Fibreno (FR, Lazio)	Soil	INGV-INSN
15	PTRL	43.442	12.438	750	CRn, iT	Pietralunga (PG, Umbria)	Indoor	IRON
16	ROM9	41.828	12.515	110	CRn, iT	Roma-Sede INGV (RM, Lazio)	Shelter	INGV-INSN
17	ROM92	41.828	12.515	110	CRn, iT	Roma-Sede INGV (RM, Lazio)	Soil	INGV-INSN
18	SPI	41.441	13.980	167	CRn, iT	San Pietro Infine (CE, Campania)	Cavity	IRON
19	SSFR	43.436	12.782	750	CRn, iT	Montelago - fr. Sassoferrato (AN, Marche)	Borehole	INGV-INSN
20	BSSO	41.546	14.594	1010	CRn, iT, iP, iRH%	Busso (CB, Molise)	Borehole	INGV-INSN
21	CERA	41.598	14.018	800	CRn, iT, iP, iRH%	Cerasuolo (IS, Molise)	Borehole	INGV-INSN
22	CEL	38.260	15.894	702	CRn, iT, iP, iRH%	Celeste (RC, Calabria)	Borehole	INGV-INSN
23	CAR1	39.253	16.521	680	CRn, iT, iP, iRH%	Carolei (CS, Calabria)	Borehole	INGV-INSN
24	PTQR	42.022	13.401	957	CRn, iT,iRH%	Pietraquaria – Avezzano (AQ, Abruzzo)	Shelter	INGV-INSN
25	SANB	42.006	13.623	687	CRn, iT, iRH%	San Benedetto dei Marsi (AQ, Abruzzo)	Borehole	IRON
26	TRAQ	41.957	13.536	685	CRn, iT, iRH%	Trasacco (AQ, Abruzzo)	Borehole	IRON:

TABLE 1. Radon monitoring sites belonging to IRON. CRn - Radon concentration, iT - internal temperature, iP - internal pressure, iRH% - internal relative humidity (per cent).

vestigate whether the fluctuations in soil radon emanation can be associated with local seismicity, in the sense of a physical correlation with the preparation process of an earthquake. In this respect, the IRON goal is to reach a fairly complete coverage of the whole Italian region. Preliminary scientific results have been obtained by means of a long term, continuous radon monitoring experiment in a seismically active area located in Umbria, a region in the northern Italian Apennines, affected by an intense micro seismic activity [Piersanti et al., 2015] and by monitoring variations in radon emissions during the 2012 Pollino sequence, in the Calabrian Apennine [Piersanti et al., 2016] and the 2016 Amatrice Norcia Visso sequence in the central Apennines [Cannelli et al., 2016].

All data recorded by IRON stations, together with installation details and instruments technical features, are stored in a specifically designed relational database, IRON-DB, hosted on a virtual server platform operated by the INGV IT services [Cannelli, 2017].

2.1 INSTALLATION TYPES

We have implemented three main installation types, in all of which soil gases reach the instrument passively (Figure 3):

i) the instrument is located in the basement of a building, typically in a closed technical room not usually accessed by people ("Indoor" in Table 1);
ii) the instrument is co-located in a small shelter with a seismic and/or geodetic station belonging to another monitoring network ("Shelter" in Table 1);
iii) the instrument is installed in a small (< 2 m deep) borehole, sometimes co-located with a seismic sensor belonging to another monitoring network ("Borehole" in Table 1).

One station (SPI) has been installed with the instrument located in a tunnel of the Acqua Campania aqueduct ("Cavity" in Table 1). In addition to scenarios listed above, four stations (BADI2, MCEL, POFI and ROM92) have been installed in environments where soil gas reaches the instrument passively from a probe partly deepened into the soil ("Soil" in Table 1).

Different installation types raise some questions about the measurement methodology. As radon easily enters indoor environments by diffusive and mainly advective migration from radon-rich subsoil, an essential requirement for "indoor" installations is that the site is in an isolated building, not influenced by anthropogenic

FIGURE 3. Some of the installation types employed in IRON: a) shelter (CDCA station), b) small borehole (MURB station) and c) soil (BADI2 station).

FIGURE 4. From a) to e): High efficiency radon monitors employed in IRON network, designed in collaboration with the Department of Nuclear Engineering and Conversion of Energies of University of Rome "La Sapienza" and manufactured by Tecnosabina. The original version of the instrument is shown in a); the current, updated version is shown in b) and c). In d) and e) the experimental version with an Arduino-Based DAQ Prototype is shown. In f) and g) the commercial radon detectors Airthings Corentium Plus and Algade Aer, respectively.

activities and without any kind of opening and/or aeration system. Fulfilling such requirements, allows indoor type stations to record data that are suitable for significant geophysical investigations [Piersanti et al., 2015; 2016]. Nevertheless, when analysing time series recorded by "shelter/borehole" stations, it is immediately evident that much smaller noise and external perturbations affect data compared with those associated with "indoor" ones (see Section 3 for details). Indeed, for the former configuration, the influence of not diurnal temperature and pressure variations are greatly reduced, and this allows to more efficiently quantify (and possibly remove) the impact of other important variables, such as precipitations, in favour of a better understanding of radon emission dynamics and more easily identifying and highlighting potential anomalies. For these reasons, we are gradually phasing out the "indoor" installation type in favour of "shelter/borehole/soil" ones for newer stations.

2.2 INSTRUMENTATION

Most IRON stations adopt a high sensitivity proprietary instrument employing an alpha scintillation detector (a Lucas Cell) consisting of a flask, whose inner wall is coated with silver-activated zinc sulphide (ZnS). It integrates a front-end electronics and measures radon concentration by counting the radon decay signals within an adjustable acquisition window (Figure 4, from a) to e)). Radon enters the detector by diffusion through an inlet filter that traps radon daughters. For 500 mL scintillating flasks, Algade ™, sensitivity is typically in the range 0.24 - 0.28 Bq m^{-3} per imp h^{-1}, while minimum detectable concentration is 3 - 6 Bq/m^{-3}. As shown in Figure 5, measured concentrations do not depend on absolute humidity. The instrument is powered by a 12V lead-acid battery, which is charged by a power supply connected to 220V mains or to a solar panel, depending also on installation types. Simultaneously with

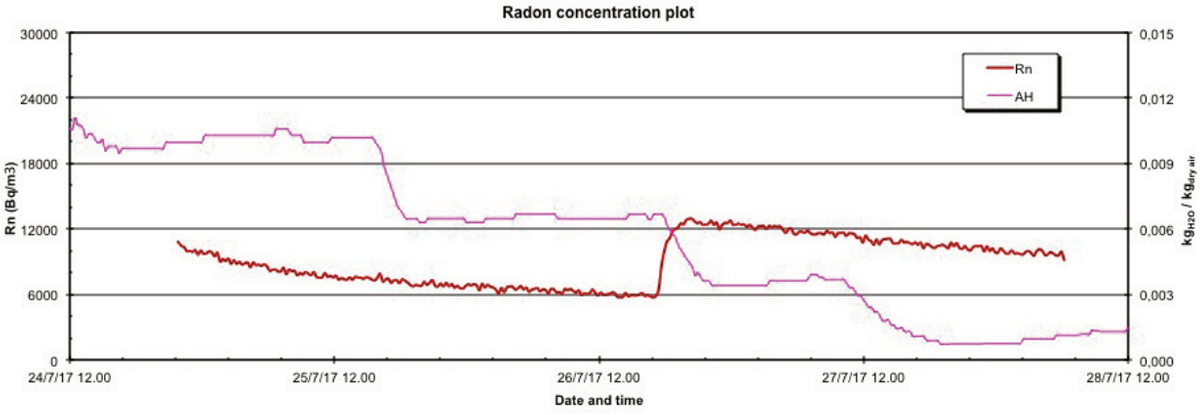

FIGURE 5. Characterization of radon proprietary instrument employed in IRON network (see Figure 4a). Radon concentration (Rn) does not depend on the absolute humidity (AH). We express humidity as absolute, instead of relative, since the amount of water in the detection volume has a dramatic relevance for radon daughters collection onto the detector and their full energy detection. The only variation in the plot (on 26/7/17 at about 18.00), apart from the decay trend, refers to enrichment in the radon chamber, just to raise the counts for a better statistical approach.

radon concentration data, stations acquire local temperature values by means of a specific sensor co-located with the radon detector. Data is stored locally in the front-end electronics memory and can be downloaded through a serial interface. We are developing a new multiparametric acquisition system with remote transmission based on the open-source Arduino platform; this low-cost, low-power data acquisition prototype is able to simultaneously record radon concentration, temperature, atmospheric pressure and precipitation, and can provide both local storage on a flash memory and real-time data transmission via the GSM network. Presently, the MCEL station is equipped with a commercial Barasol MC2 probe [Papastefanou, 2002]. The Barasol MC2 probe is used for passive measurements of radon in the ground; soil gas enters a detection volume through three cellulose filters that trap all the solid radon daughter products. The Barasol sensor is based on an implanted silicon detector with a depleted depth of 100 μm and 400 mm^2 of sensitive area; counting is made by alpha spectrometry from decays of ^{222}Rn and its daughter products created in the detection volume. The sensitivity is 50 Bq m^{-3} per imp h^{-1}. It is designed to be used in environments where the utility grid and/or solar power supply are not available, guaranteeing one year of operating time with two DD alkaline batteries, and integrates the acquisition electronics and a local memory. The probe also records temperature and atmospheric pressure. In addition to the Barasol MC2 probe, we are also operating some new stations (BSSO, CERA, CEL, CAR1, PTQR, SANB and TRAQ) equipped with the Algade Aer Plus (http://aer.dosirad.algade.fr/) and Airthings Corentium Plus (https://airthings.com/) commercial solid state radon detectors (Figure 4f) and 4g)), providing also relative humidity and, the latter, pressure sensors.

It is worth noting that the sensitivity of the proprietary instrument based on Lucas cell is two orders of magnitude higher with respect to the Barasol probe and to all other instruments equipped with solid state detectors, and that its operation does not depend on soil/air absolute humidity. On the other hand, it requires an external power supply, it consumes more power and it is more vulnerable to aggressive pollutants; these aspects may represent strict limitations when planning new installations.

3. PERFORMANCE OF RADON MONITORING NETWORK

Figures 6.1, 6.2 and 6.3 show raw time series recorded at stations operating for at least one year (18 out of 26 total stations), whilst the corresponding long-term radon variations are given in Table 2. Sites with longer time series, as CTTR (Figure 6.1) - MMN (Figure 6.2) - PTRL (Figure 6.3), show a clear seasonal signal, likely connected with temperature fluctuations, to which "indoor" installations seem to be more sensitive. This correlation between radon concentration and temperature variations is less evident, for example, at CDCA and MURB sites, where "shelter" and "borehole" installations, respectively, reduce the influence of this meteorological parameter on soil radon emanation. A specific example of this behaviour is shown in Figure 7, where radon emission time series, recorded at an indoor (PTRL) and

Code	Operating from	Length of ts (days)	Avg	Min	Max	Availability (%)
BADI	2014	787	466	291	2769	99
BADI2	2015	45	1142	310	1994	100
CAE	2015	392	1788	332	11732	65
CDCA	2014	1007	321	41	6773	100
CMPL	2009	2849	4883	290	15977	39
CTTR	2010	2636	1001	69	3370	98
FRME	2013	1306	623	206	5344	89
GALL	2015	790	719	158	8328	99
MMN	2011	2011	1728	72	17024	99
MMNG	2012	1681	796	110	4546	81
MURB	2013	1118	256	61	5651	93
NRCA	2016	117	897	468	3966	98
POFI	2013	25	426	1015	48	64
PTRL	2010	1932	1301	268	4665	91
ROM9	2014	279	1238	199	28158	99
ROM92	2014	279	7206	251	17970	99
SPI	2016	42	9703	438	27061	100
SSFR	2013	1021	3994	169	42623	87

TABLE 2. Statistics of radon time-series (ts) from 18 monitoring sites operating since at least one year. The reported length of time-series is referred to the sum of effective days of acquisition, without breaks due to technical failures or maintenance. Radon concentration is given in Bq/m3. Availability, expressed in %, represents the ratio between the actual operating time and the wall-clock time.

at a small borehole (MURB) station in a shared acquisition time-window are compared. The signal registered at PTRL (blue line) shows much greater background variability with respect to the one registered at MURB (red line). In particular, PTRL shows a clear seasonal behaviour: during the summer months (July-August) absolute radon concentration peaks of about 300-350 Bq/m^3 are observed, as a consequence of the positive correlation between radon variations and temperature. In the same period, we observe at MURB concentration peaks not exceeding 100 Bq/m^3, confirming that a station acquiring in a small closed volume (not exceeding 5 m^3) in contact with soil (small borehole) is less dependent from meteorological parameters. Consequently, in the latter case, deviation from the standard background behaviour is more easily evidenced (e.g. June 2015).

An apparently anomalous behaviour of soil radon concentration is observed from January 2017 at GALL (Figure 6.2), where the instrument has been relocated in a different room of the same building basement for technical reasons. Though our interest is mainly focused on radon transient variations and not absolute concentrations magnitude, we are gradually replacing “indoor” stations with “shelter/borehole/soil” installation types also in order to avoid these unexpected but possible situations.

So far, the relation between variations in radon emissions and seismicity has been investigated at three different monitoring sites. At PTRL, in the framework of a research infrastructure devoted to study earthquake preparatory processes and located along the upper Tiber Valley, we investigated the correlation between radon variations and a local intense micro seismic activity, highlighting the different roles played by meteorological parameters and by variations of seismic moment release in modulating the radon emanation [Piersanti et al., 2015]. At MMN, a 3-years long record of radon concentration data has been collected while a seismic sequence was active in the Pollino area, Calabria (Southern Italy) [Piersanti et al., 2016]. We developed an empirical algorithm for reducing the effects on radon fluctuations of meteorological parameters, as temperature and precipitation that are extremely local factors and play a crucial role in radon transportation in porous media and exhalation [Klusman and Webster, 1981; Inan et al., 2012]. We also tested, through a numerical analysis, the possibility of highlighting in advance the

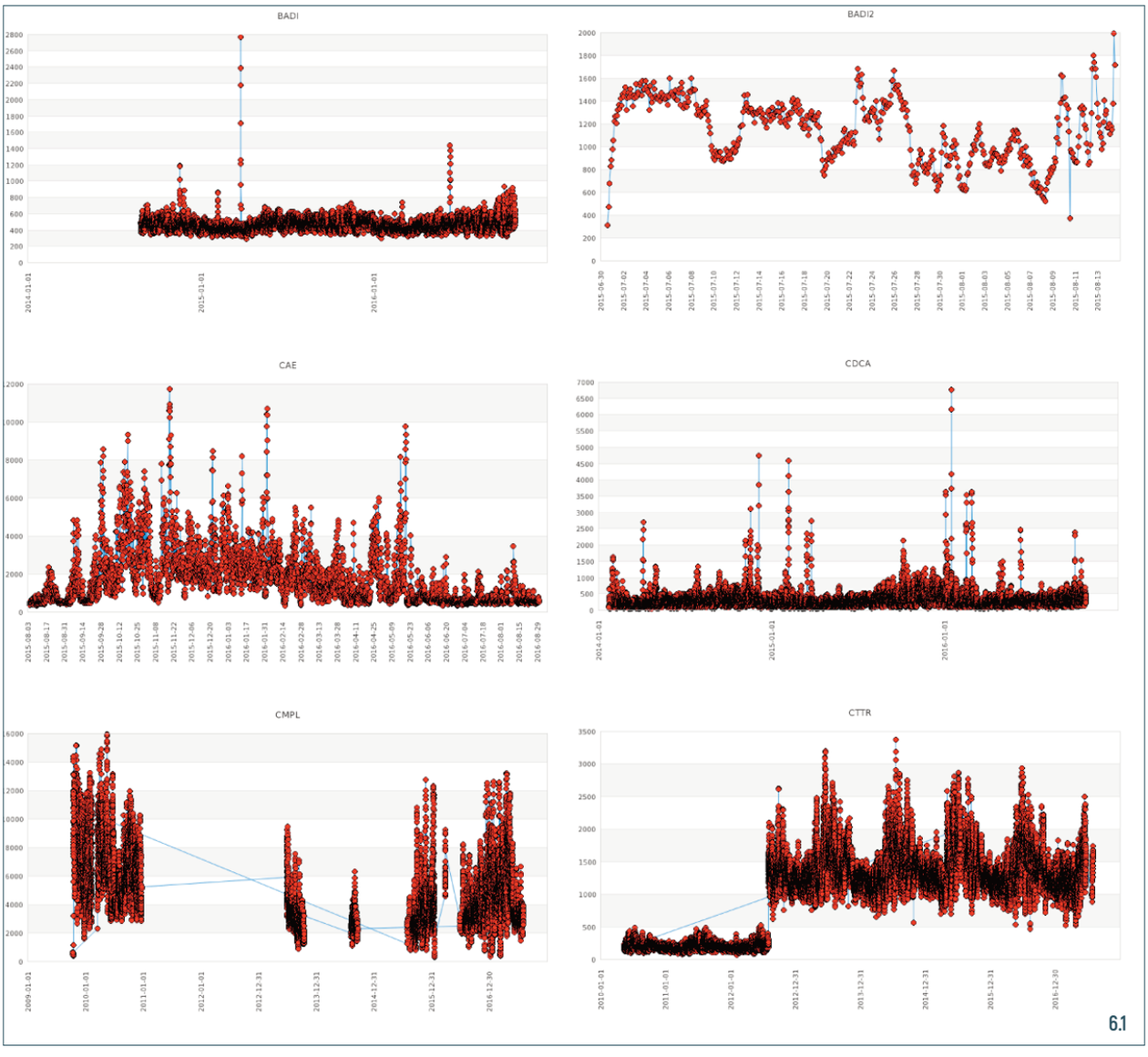

FIGURE 6. Radon (CPM) soil time-series from 18 of 26 total sites operating since at least one year, as of November 2017, split in three different panels 6.1 (BADI-BADI2-CAE-CDCA-CMPL-CTTR), 6.2 (FRME-GALL-MMN-MMNG-MURB-NRCA), and 6.3 (POFI-PTRL-ROM9-ROM92-SPI-SSFR). In the additional material each radon soil time series is available in high resolution.

occurrence of the major events of the seismic sequence. Finally, we interpreted the field data collected at CTTR for three years before the Ml=6 Amatrice earthquake [Cannelli et al., 2016]. In view of the outcome of laboratory experiments, aimed to study real time radon emission dynamics from rock samples subject to normal and shear stress loads, this analysis suggests the possibility of a minor role played by phenomena related to fluid migration in the onset of the Amatrice seismic event with respect to other recent Apennine earthquakes.

In the following we discuss the possibility of highlighting and detecting subsurface processes by means of their fingerprint in soil radon emissions. Specifically, we compare (i) different acquisition systems, (ii) different installation types, and (iii) the spatio-temporal occurrence of transients within the network.

3.1 PERFORMANCE COMPARISON FOR DIFFERENT INSTRUMENTS

As stated in Section 2.2, different radon monitors have been deployed in IRON stations. Cross comparison and calibration of these devices have been performed through a radon chamber facility available at INGV Radionuclide Laboratory. The radon chamber can be directly connected to INGV monitors and, simultaneously, to a slave chamber containing the small sized AER and Corentium monitors. The above procedure is being re-

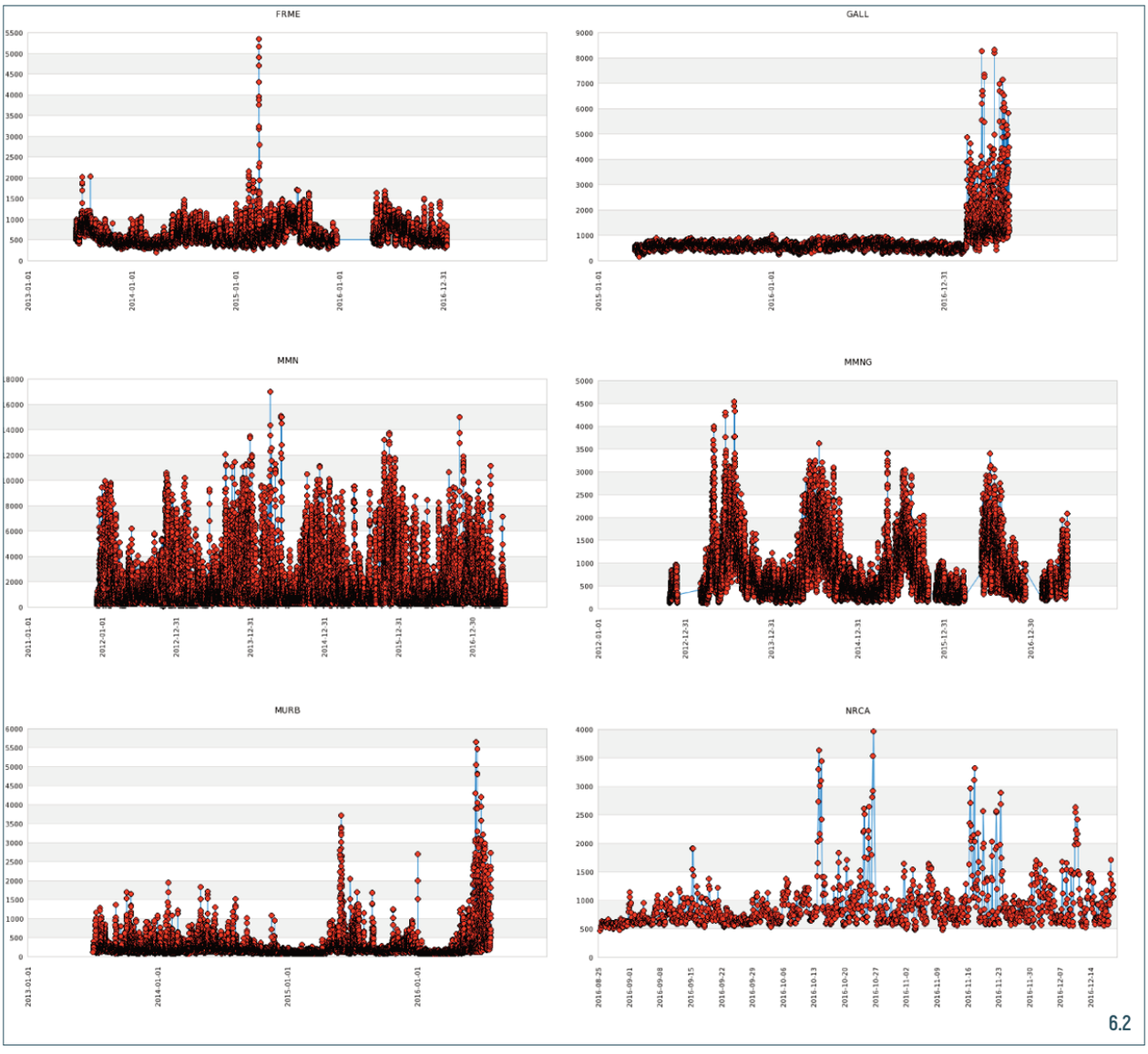

6.2

peated for every instrument, before its installation in IRON stations.

The details of the calibration protocol will be the subject of a forthcoming technical report. Figure 8 shows a typical cross comparison result; the pale blue line represents the radon concentration trend in the main chamber, when the equilibrium condition after radon diffusion toward the slave chamber and inside the monitor detection volumes has been reached.

Radon concentrations recorded by INGV (brown line), AER (blue line) and Corentium (red line) detectors after calibration follow the ideal trend remarkably well. Nonetheless, signal variability is higher in the AER and Corentium instruments with respect to that showed by the INGV detector. This difference, which is independent from the specific acquisition time window (15 min AER and INGV, 1h Corentium), is due to the different sensitivities of the instruments (low sensitivity for the AER and Corentium monitors, high sensitivity for the INGV instrument). As a matter of fact, a trade off exists between acquisition time, detector sensitivity and error associated to the measure, which has to be taken into account when planning station deployments. Counts obtained from nuclear decays follow Poisson distribution, consequently the best uncertainty estimation is given by the standard deviation of the distribution, i.e. by the square root of the recorded counts (C),

$$\sigma_c = \sqrt{C} = \sqrt{T_{acq} \cdot CPM}$$

where T_{acq} and CPM are the acquisition time and the counts per minute, respectively. Therefore, relative error σ_C/C can be reduced by increasing T_{acq} and/or CPM. CPM obtained with the INGV monitor for a given radon concentration are around 25 to 70 times greater (depending on the scintillation cell size) than that exhibited by the other employed detectors and 50% response being as fast as.

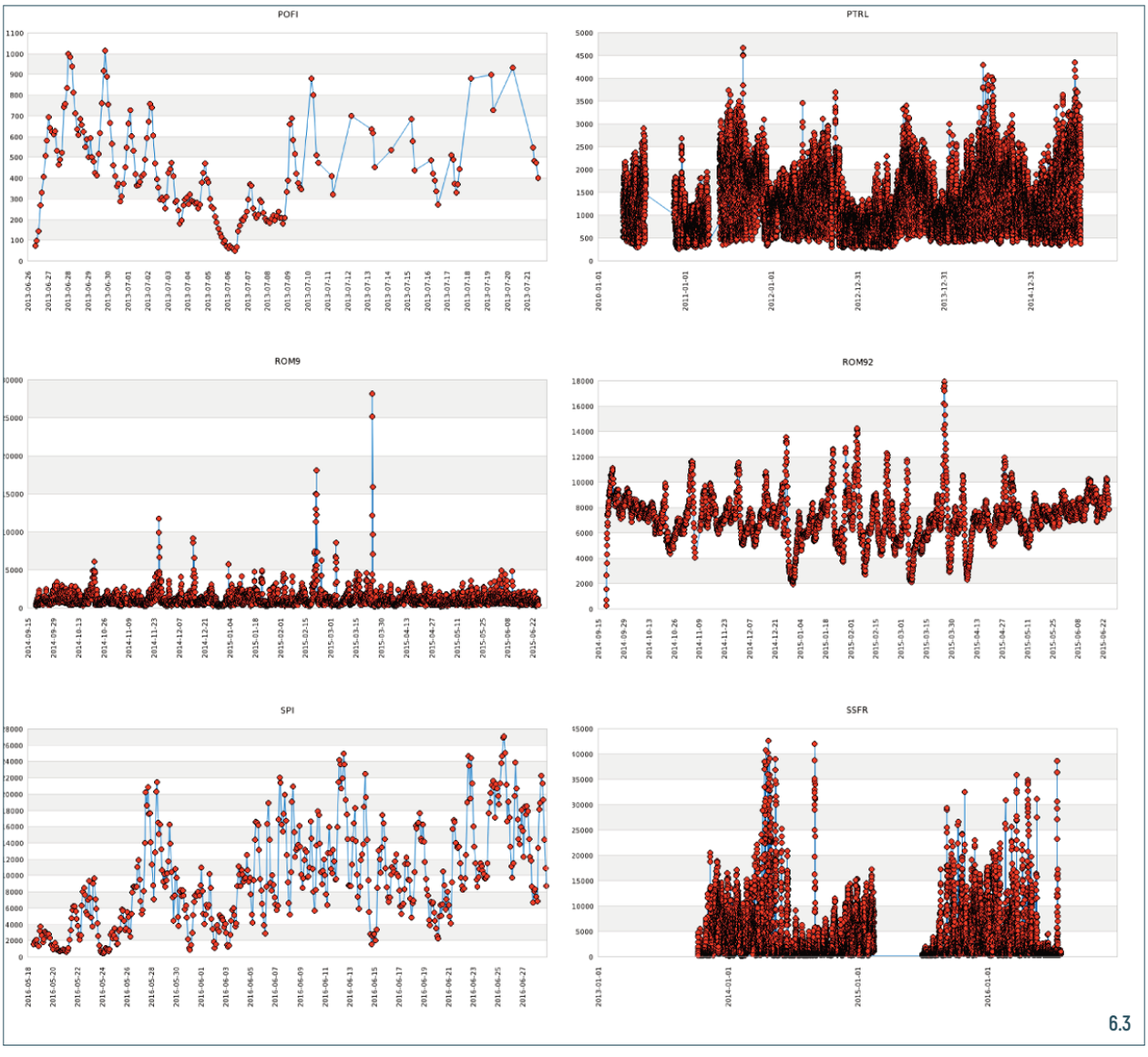

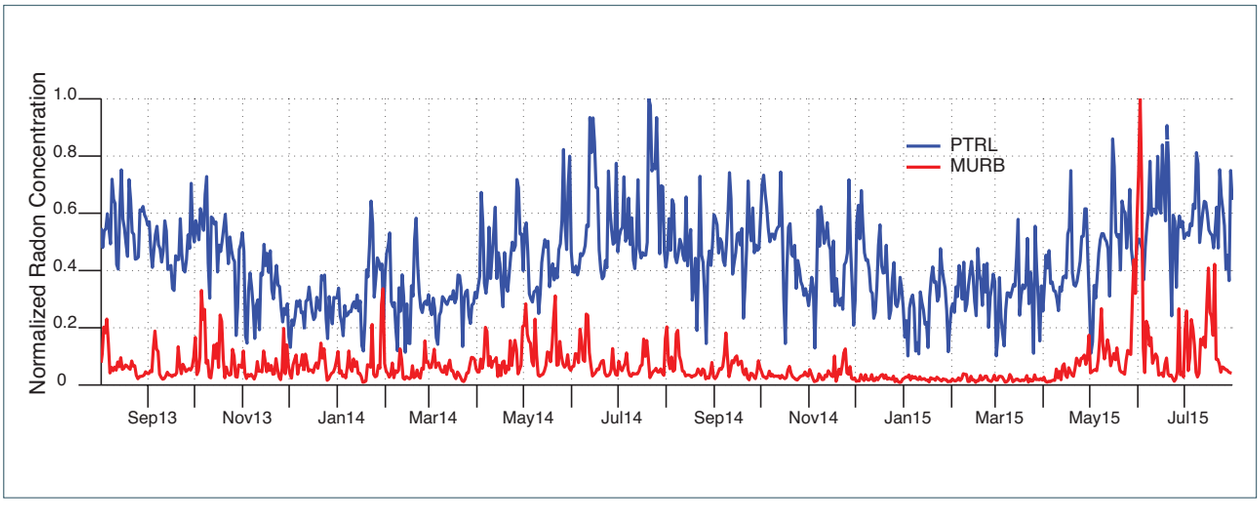

FIGURE 7. Daily radon concentration time series from PTRL (indoor) and MURB (small borehole) stations, during the period from August 2013 to August 2015. Each time series has been normalized to its maximum value of radon concentration found in the selected time-window.

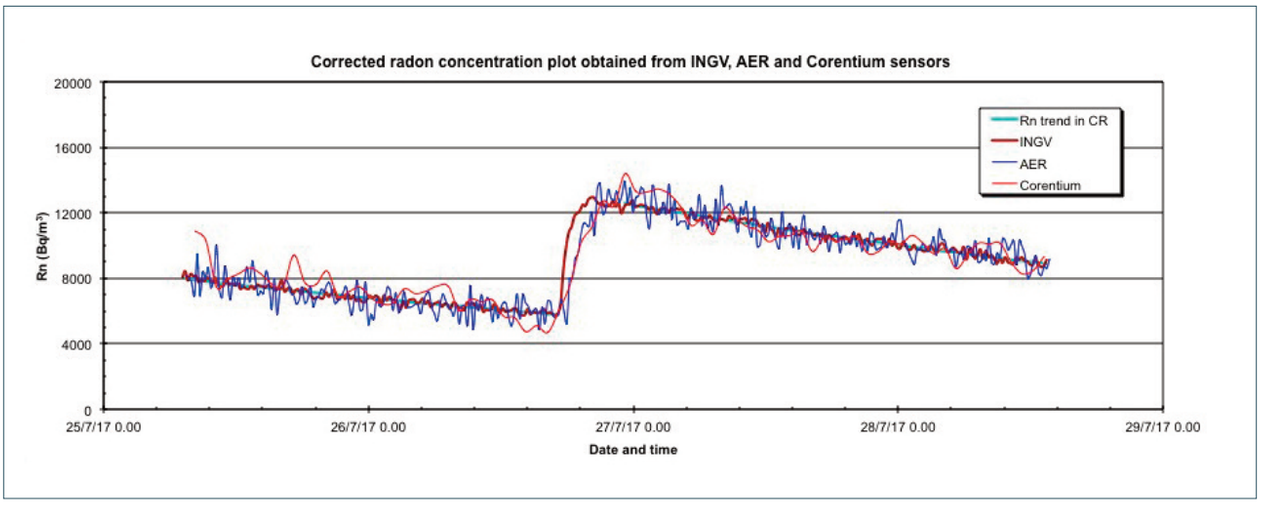

FIGURE 8. Cross comparison of corrected radon concentration acquired by INGV (brown line), AER (blue line) and Corentium sensors (red line). The pale blue line represents the radon concentration trend in the main chamber when the equilibrium condition after radon diffusion toward the slave chamber and inside the monitor detection volumes was reached.

3.2 SHELTER VS. SOIL PROBE INSTALLATION TYPE: BADI AND BADI2

BADI and BADI2 stations were installed in August 2014 and June 2015, respectively, at Badiali (PG, Umbria). The stations are located in a small shelter, belonging to the INGV-INSN network and hosting the BADI homonymous seismic station. They represent a couple of twin stations acquiring simultaneously the same radon signal, with BADI being a shelter installation and BADI2 a soil installation (see Table 1). This experiment was performed in order to compare acquisitions obtained employing two different installation types in the same conditions and in the same place (the instruments are installed within a distance of 2 m) and therefore, potentially influenced by the same local meteorological factors. Figure 9 shows radon concentration simultaneously recorded at BADI and BADI2 during the month of July 2015, representing only the shared acquisition time-window, since data acquisition at BADI2 has stopped on 18/05/2015 because of a technical failure, and the station has been offline until 25/10/2016. Apart from the difference in the absolute magnitude, the two signals show remarkably similar correlating features. Similar results have been achieved in a similar experiment comparing the signals recorded by ROM9 and ROM92 [see Appendix A in Piersanti et al., 2015]. Again, the two signals were remarkably correlated but in that case the soil probe approach exhibited a slightly lower dynamic range [Figure 1A in Piersanti et al., 2015]. Indeed, ROM9 and ROM92 were placed in an area characterized by quite high radon emanation levels, while exactly the opposite holds for BADI and BADI2. Nevertheless, both experiments allow us to conclude that results obtained with an "indoor" setup are equivalent with respect to those obtained measuring radon concentration drawing soil gas from a probe inserted directly into the soil, provided that the accumulation chamber is sufficiently small (small borehole or shelter). The soil probe approach gives a higher signal-to-noise ratio for transient signals, which can be a critical factor when the sensitivity of the detection system is a key feature (for example, in case of very low levels of radon emanation). The "indoor" approach, on the other hand, shows great variability in the range of the observed signal at the expense of a loss in the absolute magnitude, not representing a problem when high sensitivity equipment is used.

3.3 ON THE LOCALITY OF IMPULSIVE TRANSIENTS IN RADON CONCENTRATION: CDCA AND BADI

CDCA and BADI stations, both shelter-type installations (Table 1), were installed in January and August 2014, respectively. CDCA is co-located with the homonymous seismic station of INGV-INSN, whose sensor is placed in a borehole at a depth of about 70 m. The pipes (10 cm in diameter) containing signal cables from the seismometer to the acquisition electronics are used to circulate air between the bottom of the borehole and the radon detector placed at surface. This approach, while cannot be as effective as a proper borehole installation, nevertheless allows to measure radon concentrations representative of the situation at depth. Details of BADI have been discussed above. The two stations are about 6 km away from each other,

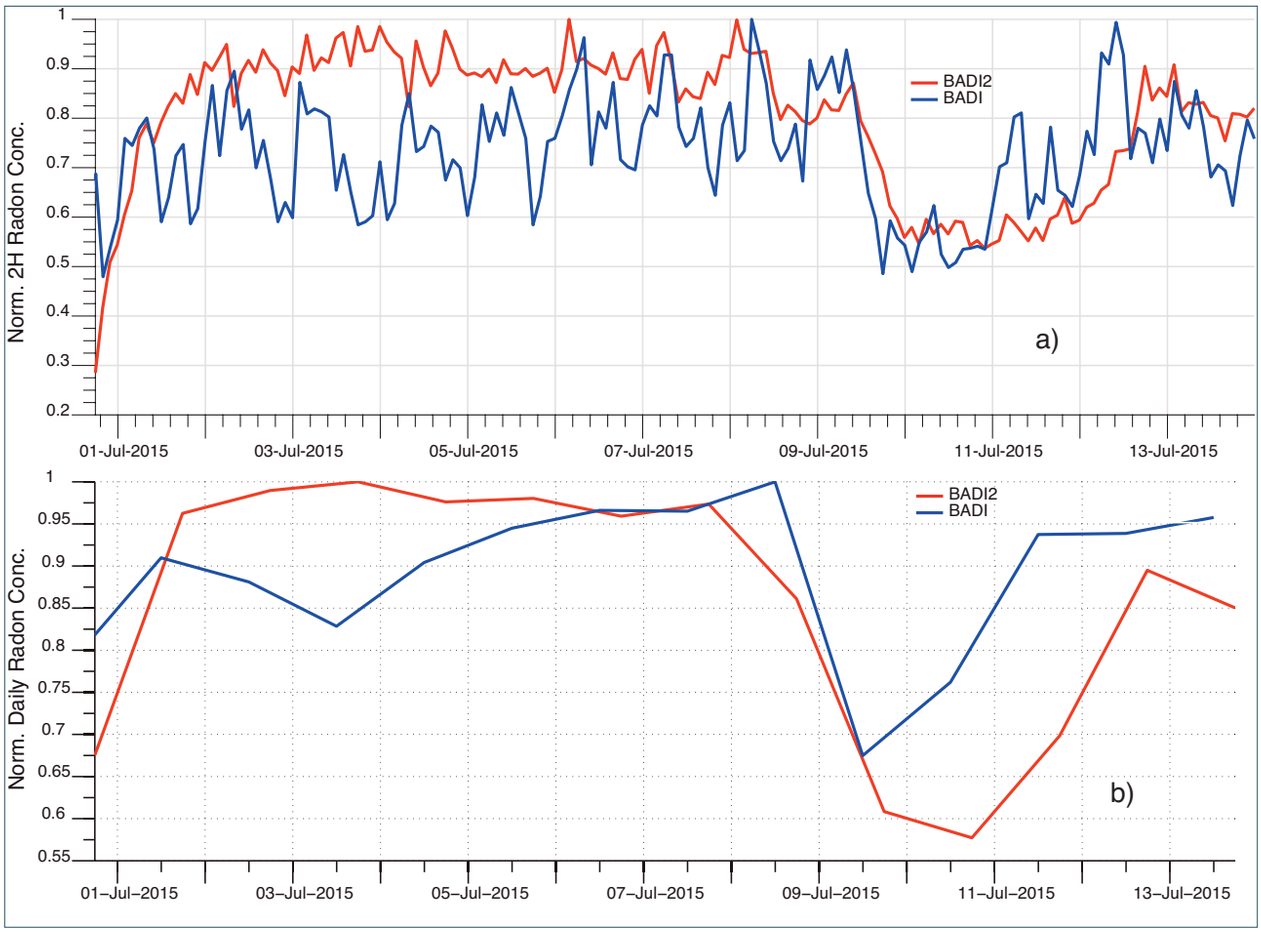

FIGURE 9. 2-Hours (a) and daily moving averaged (b) time series of the radon concentration from BADI (blue line) and BADI2 (red line) stations during the period from 1 July until 13 July 2015. Each time series has been normalized to its maximum value of radon concentration found in the selected time-window. In panel a) concentration peak values for BADI and BADI2 are equal to 59 Bq/m^3 and 1524 Bq/m^3, respectively. In panel b) concentration peak values for BADI and BADI2 are equal to 49 Bq/m^3 and 163 Bq/m^3, respectively.

sharing therefore some common meteorological influences, while others (like precipitation) could be distinct for the two sites. The comparative analysis of the signals recorded at CDCA and BADI stations give us some important insights about the remote origin of the signal: both stations are characterized by a low and stable background signal (Figure 10), compared to other stations (see for example MURB in Figure 6.2 or SSRF in Figure 6.3), indicating a minor sensitivity of these two sites to temperature and atmospheric pressure variations. Both CDCA and BADI time series exhibit few sharp and marked increases in radon emanation lasting from one to few days. Thanks to the low and stable background signal, this feature is particularly evident in BADI, but still perfectly detectable in CDCA. Almost all impulsive signals recorded at BADI occur in the same (or adjacent) day also at CDCA, with the exception of four spikes occurring only at CDCA site in the period from January to March 2016. If the variations in radon concentrations recorded at BADI station were due to very local sources, it would be hard to explain why these impulsive signals are recorded also at CDCA station (and vice versa). Indeed, to our knowledge, impulsive signals of such magnitude have never been successfully associated to a meteorological forcing in literature. By applying the empirical procedure described in Piersanti et al. [2016], we were not able to correct those signals, no matter the correction parameters we adopt. One viable explanation is that a single internal phenomenon is modulating the radon signal recorded at both stations. Indeed, Tommasone et al. [2015] highlighted an apparently similar effect as a consequence of rainstorms. Nevertheless, a more thorough comparison shows that in Tommasone et al. [2015] a radon rich alluvial soil has been monitored; and, after rainstorm episodes, a sudden increase in radon concentrations by a factor 1.5-2, lasting 2 to 6 hours is followed by a sharp drop by a factor 10 or more. The spikes

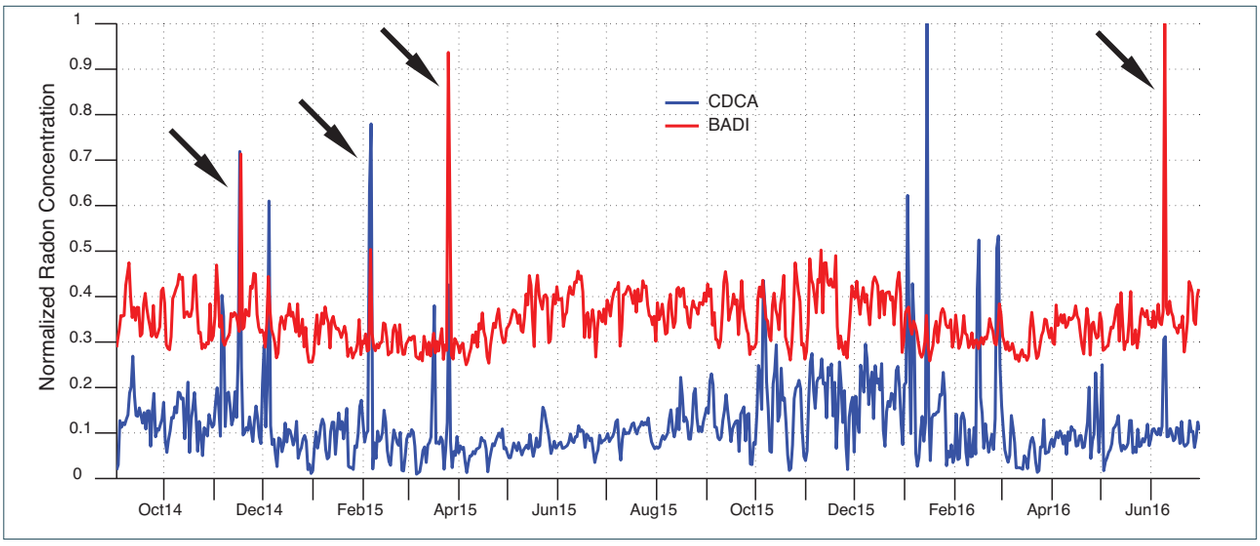

FIGURE 10. Daily radon concentration time series from CDCA (blue line) and BADI (red line) stations (both of them are shelter-type installations), during the period from September 2014 to June 2016. Each time series is normalized to its maximum value of radon concentration found in the selected time-window. Black arrows highlight radon emanation peaks occurring simultaneously at both stations.

observed at CDCA and BADI last significantly more (from 6 to 20 hours) and, most of all, after the sudden increase, at CDCA and BADI, radon concentrations go back to usual background levels, without the further sharp dropping observed by Tommasone et al. [2015] as a consequence of rainstorm. Indeed, the overall radon dynamics observed after rainstorm episodes by Tommasone et al. [2015] is in substantial agreement, on daily timescales, with that observed by Piersanti et al. [2016] in similar meteorological conditions. The short-time increase before dropping observed by Tommasone et al. [2015] could be related to their high frequency resolution or to the peculiar geological features of their testing site (radon very rich alluvial deposits) or, most likely, a mix of the two.

4. CONCLUSIONS

The IRON network is aimed at developing a national network of high-resolution permanent real time radon monitoring stations, whose purpose is the research about multi-scale physical processes controlling faulting earthquake generation. An essential requirement for a radon monitoring network to be an effective research tool in seismotectonics is the ability to provide long-term records of data. Indeed, the main limitation when trying to associate radon measurements with Earth's internal processes is the difficulty of ruling out the possibility that observed variations are due to environmental effects, such as meteorological parameters, and/or random noise because seismo-tectonically and meteorologically induced radon anomalies may look strikingly similar. It is converging evidence that meteorological parameters generally play an important role in modulating soil radon emanations. Even the relative importance among the main relevant variables (temperature, precipitation, pressure) in modulating the radon emissions cannot be uniquely determined and it is likely to be site dependent, since different analyses led to different results. In Piersanti et al., [2016] we developed an empirical correction procedure to take into account (i.e. remove, or at least reduce) the effect of meteorological parameters (temperature, pressure and precipitation variations) on the radon measured concentration. This aspect is mandatory to grant that long-term signal modulations and noise characteristics can be properly evaluated. We addressed this issue by implementing a dense, permanent network with coherent installation protocols, which results in systematic, homogeneous measurements, with a total of 26 permanent stations installed to date (mostly longer than 4-5 years). This approach goes far beyond the simpler and widely attempted "one to one" association between a single radon anomaly detected by a single station and a specific earthquake (that is intrinsically less robust). Additionally, our strategy offers the possibility to study the behaviour of radon emanation evolution under controlled conditions, since standardized shelter and borehole installation types grant steady and predictable features in the recorded time series. Several IRON stations are co-located with INGV-INSN stations that con-

tain seismometers, accelerometers and often GPS instrumentation. This ideally guarantees a multi-parametric, multi-site and multi-level long term measurement approach. The relational database IRON-DB i) allows access to all the collected data, as well as instrumentations and different type of installations and, ii) keeps track of the evolution of the network. It is currently reachable only from the internal computer network of INGV, however in the near future it will be linked to a public web interface to ensure data dissemination.

Acknowledgements. We warmly thank H. Woith and an anonymous reviewer for their careful reviews that helped to improve our manuscript. Some figures have been drawn using the Generic Mapping Tools (GMT) of Wessel and Smith [1998].

REFERENCES

Abbady et al. 2004. Abbady, A., Abbady, A. G. E., and Michel, R.: Indoor radon measurement with The Lucas cell technique, Appl. Radiat. Isotopes, 61 (2004), 1469–1475.

Cannelli et al., 2016. Cannelli V., Piersanti A., Spagnuolo E., Galli G., Preliminary analysis of radon time series before the Ml=6 Amatrice earthquake: possible implications for fluid migration, Annals of Geophysics, [S.l.] (2016), http://dx.doi.org/10.4401/ag-7166.

Cannelli, 2017. IRON-DB: a database for the Italian Radon mOnitoring Network, Rapporti Tecnici INGV, n.371 2017, http://www.ingv.it/editoria/rapporti/2017/rapporto371/.

Chiaraluce et al., 2014. Chiaraluce L., Amato A., Carannante S., Castelli V., Cattaneo M., Cocco M., Collettini C., D'Alema E., Di Stefano R., Latorre D., Marzorati S., Mirabella F., Monachesi G., Piccinini D., Nardi A., Piersanti A., Stramondo S.,Valoroso L.,The Alto Tiberina Near Fault Observatory (northern Apennines, Italy). Annals of Geophysics, vol.57, n.3. (2014) http://dx.doi.org/10.4401/ag-6426.

Hauksson, E. & Goddard, J.G., 1981. Radon earthquake precursor studies in Iceland, Journal of Geophysical Research, 86, 7037-7054.

Inan, S. & Seyis, C., 2010. Soil radon observations as possible earthquake precursors in Turkey, Acta Geophys., 58, 828-837, doi: DOI 10.2478/s11600-010-0010-0.

Inan et al., 2012. Inan, S., A. Kop, H. Cetin, F. Kulak, Z. Pabuccu, C. Seyis, S. Ergintav, O. Tan, R. Saatcilar and M.N.

Bodur (2012). Seasonal variations in soil radon emanation: long-term continuous monitoring in light of seismicity, Nat. Hazards, 62 (2), 575-591; http://dx.doi.org/10.1007/s11069-012-0096-6.

Jaishi et al., 2014. H.P. Jaishi, S. Singh, R.P. Tiwari, R.C. Tiwari (2014). Correlation of radon anomalies with seismic events along Mat fault in Serchhip District, Mizoram, India, Applied Radiation and Isotopes, 22. doi:10.1016/j.apradiso.2013.12.040.

Klusman R.W., and J.D. Webster (1981). Preliminary analysis of meteorological and seasonal influences on crustal gas emission relevant to earthquake prediction, B. Seismol. Soc. Am., 71, 211-222.

Lewicki et al., 2014. Lewicki, J. L., Hilley, G. E., Shelly, D. R., King, J. C., McGeehin, J. P., Mangan, M., and Evans, W. C.: Crustal migration of CO2-rich magmatic fluids recorded by tree-ring radiocarbon and seismicity at Mammoth Mountain, CA, USA, Earth Planet. Sc. Lett., 390 (2014), 52–58.

Miller et al., 2004. Miller, S.A., Collettini C., Chiaraluce L., Cocco M., Barchi M. R., Boris J. P. K., Aftershocks driven by a high pressure CO2 source at depth, Nature, 427 (2004). http://dx.doi.org/10.1038/nature02251.

Mollo et al., 2011. Mollo, S., Tuccimei, P., Heap, M. J., Vinciguerra, S., Soligo, M., Castelluccio, M., Scarlato, P., Dingwell, D. B., Increase in radon emission due to rock failure: An experimental study, Geophysical Research Letters, 38, 14 (2011). http://dx.doi.org/10.1029/2011GL047962.

Ordinanza del Presidente del Consiglio dei Ministri (OPCM) (2006) Criteria for the identification of seismic zones for the production and updating of lists of the aforementioned zones. Ordinance no. 3519 of the 28th April 2006 (in Italian).

Papastefanou, C. 2002. An overview of instrumentation for measuring radon in soil gas and groundwaters, Journal of Environmental Radioactivity, Volume 63, Issue 3 (2002), Pages 271-283, ISSN 0265-931X, http://dx.doi.org/10.1016/S0265-931X(02)00034-6.

Piersanti et al., 2015. Piersanti, A., Cannelli, V., and Galli, G.: Long term continuous radon monitoring in a seismically active area, Ann. Geophys., 58 (2015), S0437, doi:10.4401/ag-6735.

Piersanti et al., 2016. Piersanti, A., Cannelli, V. and G. Galli, The Pollino 2012 seismic sequence: clues from continuous radon monitoring, Solid Earth, 7 (2016), 1303-1316, doi:10.5194/se-7-1303-2016.

Semkow et al., 1994. Semkow, T. M., Parekh, P. P., Schwenker, C. D., Dansereau R., and Webber, J. S. Efficiency of the Lucas scintillation cell, Nucl. Instrum. Methods A, 353 (1994), 515–518, 1994.

Shelly et al., 2015. Shelly, D. R., Taira, T., Prejean, S. G.,

Hill, D. P., and Dreger, D. S.: Fluid-faulting interactions: Fracture-mesh and fault-valve behavior in the February 2014 Mammoth Mountain, California, earthquake swarm, Geophys. Res. Lett., 42 (2015), 5803–5812.

Singh et al., 2016. Singh, S., Jaishi, H. P., Tiwari, R. P., Tiwari, R. C. A study of variation in soil gas concentration associated with earthquakes near Indo-Burma Subduction zone, Geoenvironmental Disasters, 3:22 (2016), 2197-8670, doi:10.1186/s40677-016-0055-8.

Singh et al., 2017. Singh, S., Jaishi, H. P., Tiwari, R. P., Tiwari, R. C. Time Series Analysis of Soil Radon Data Using Multiple Linear Regression and Artificial Neural Network in Seismic Precursory Studies, Pure and Applied Geophysics, 174 (2017). doi:10.1007/s00024-017-1556-4.

Stefansson, R. 2011. Advances in Earthquake Prediction, Springer-Verlag, Berlin, Heidelberg, 300 pp., doi:10.1007/978-3-540-47571-2, 2011.

Tommasone et al. (2015) Tommasone Pascale, F., Carbone, P., De Francesco, S. et al. Rainstorm-induced soil 222Rn concentration spikes observed in Southern Italy. Environ Earth Sci 73: 8177 (2015). https://doi.org/10.1007/s12665-014-3976-0.

Tuccimei et al., 2010. Tuccimei, P., Mollo, S., Vinciguerra, S., Castelluccio, M., Soligo, M., Radon and thoron emission from lithophysae-rich tuff under increasing deformation: An experimental study, Geophysical Research Letters, 37 (2010), 5. http://dx.doi.org/10.1029/2009GL042134.

Wessel, P., and W. H. F. Smith (1998), New, improved version of Generic Mapping Tools released, Eos T. Am. Geophys. Un., 79 (47), 579, doi:10.1029/98EO00426.

Woith, H, 2015. "Radon earthquake precursor: A short review", The European Physical Journal Special Topics, Volume 224, Issue 4, pp 611–627.

*CORRESPONDING AUTHOR: Valentina CANNELLI,
Istituto Nazionale di Geofisica e Vulcanologia,,
email: valentina.cannelli@ingv.it

Supplemental Material for

ITALIAN RADON MONITORING NETWORK (IRON): A PERMANENT NETWORK FOR NEAR REAL-TIME MONITORING OF SOIL RADON EMISSION IN ITALY

Valentina Cannelli[1], Antonio Piersanti[1], Gianfranco Galli[1], Daniele Melini[1]

[(1)]Istituto Nazionale di Geofisica e Vulcanologia, Roma, Italy

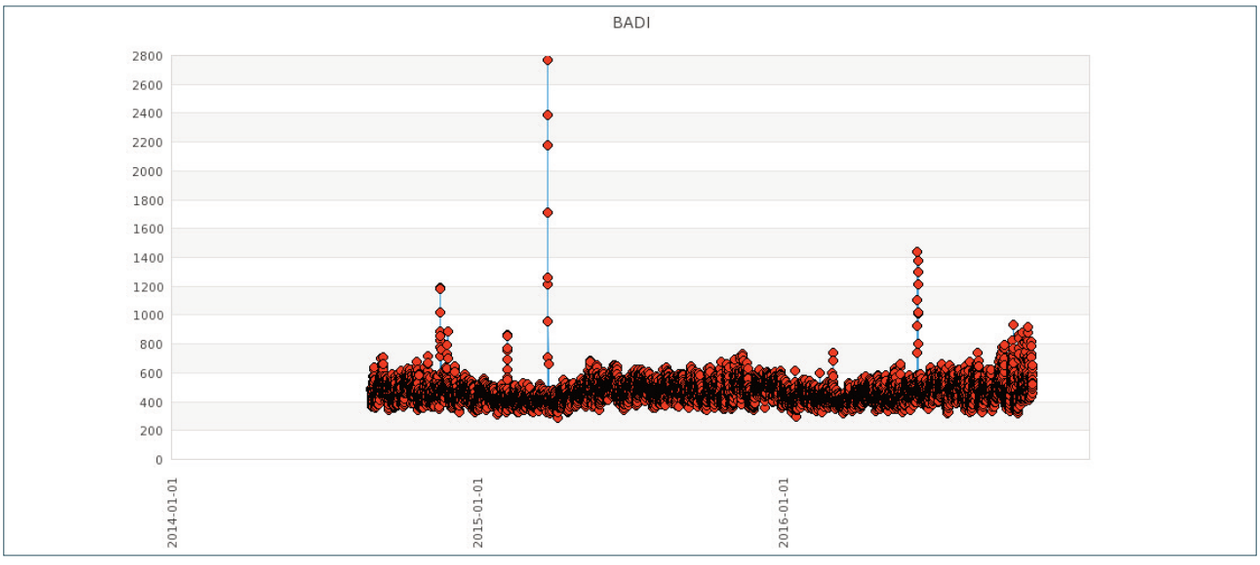

FIGURE S1. Radon (CPM) soil time-series from BADI station, as of November 2017.

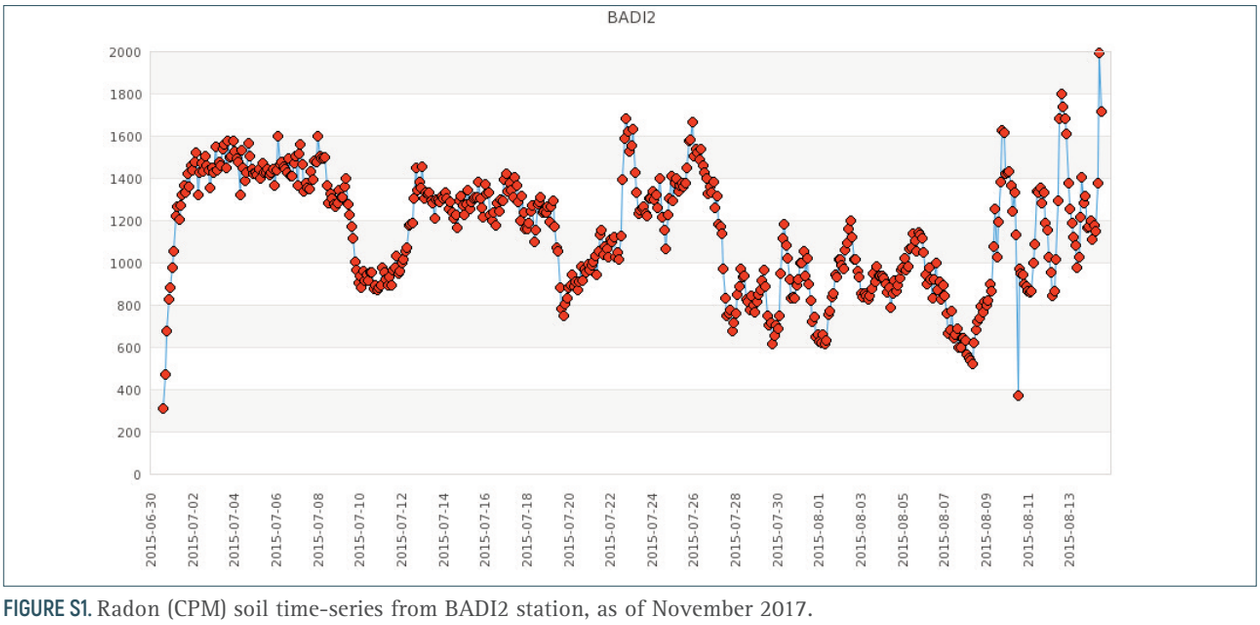

FIGURE S1. Radon (CPM) soil time-series from BADI2 station, as of November 2017.

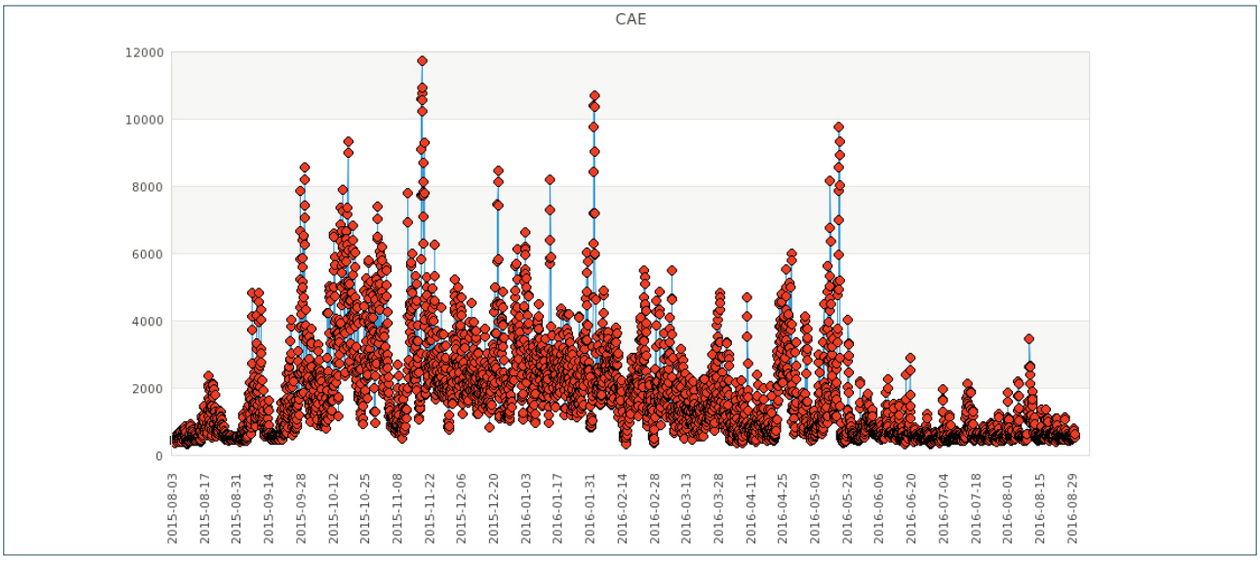

FIGURE S3. Radon (CPM) soil time-series from CAE station, as of November 2017.

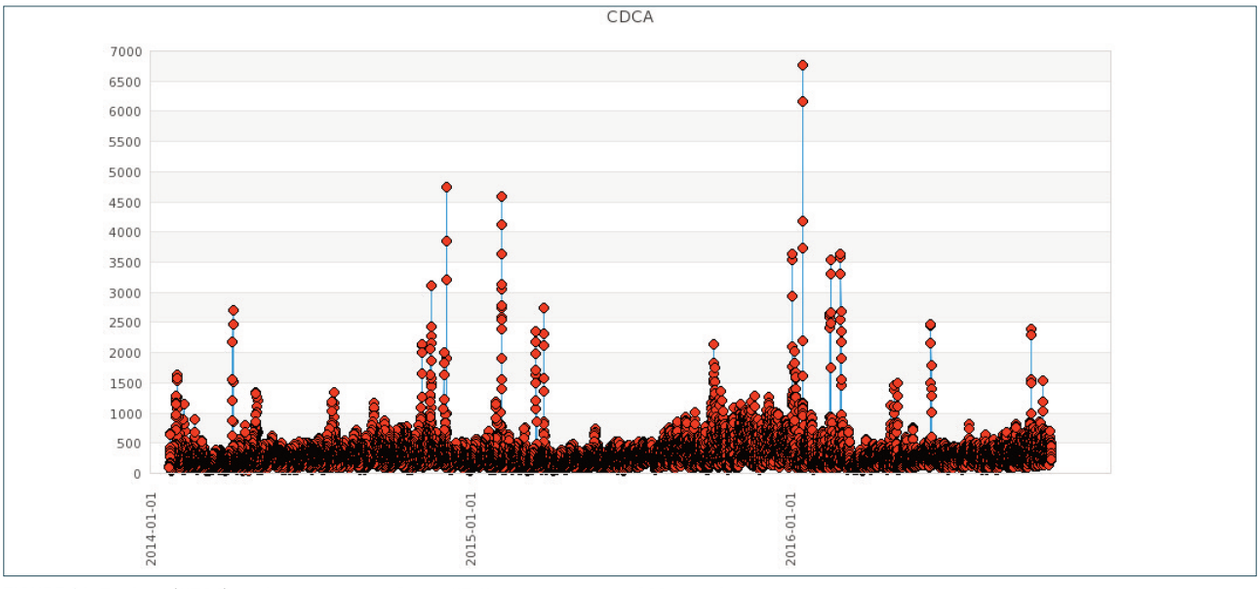

FIGURE S4. Radon (CPM) soil time-series from CDCA station, as of November 2017.

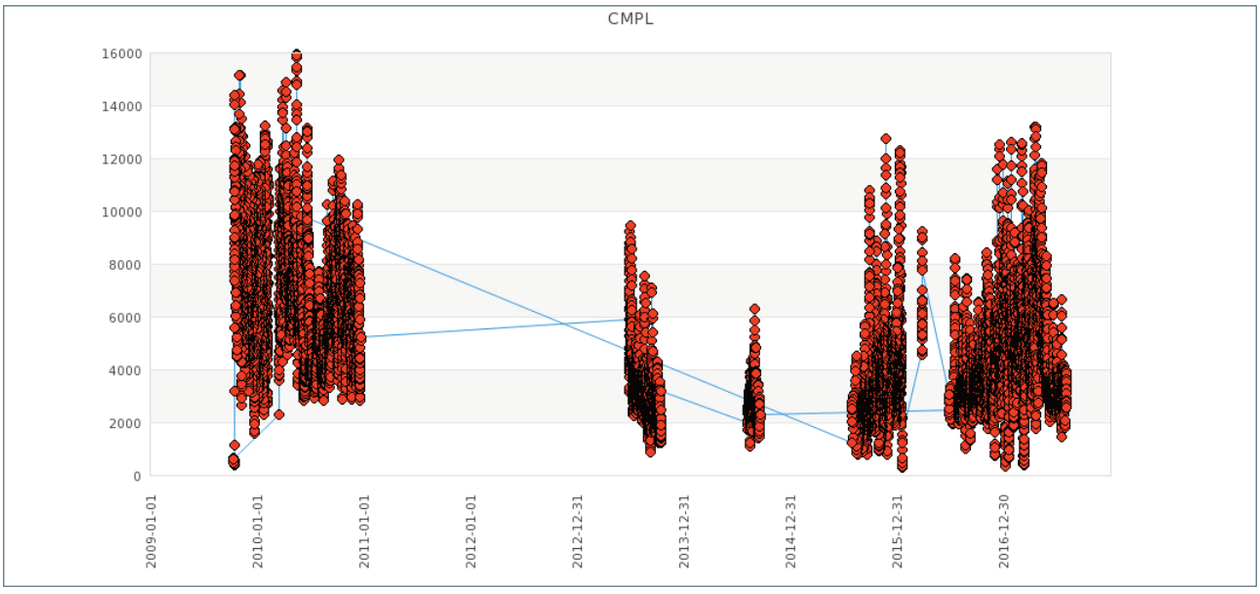

FIGURE S5. Radon (CPM) soil time-series from CMPL station, as of November 2017.

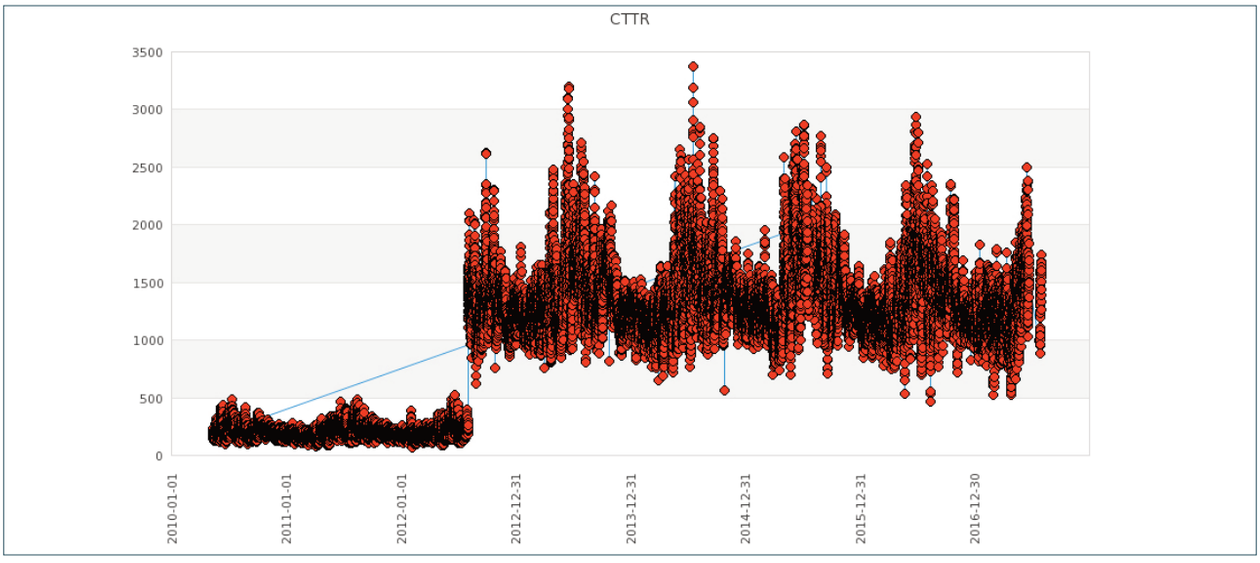

FIGURE S6. Radon (CPM) soil time-series from CTTR station, as of November 2017.

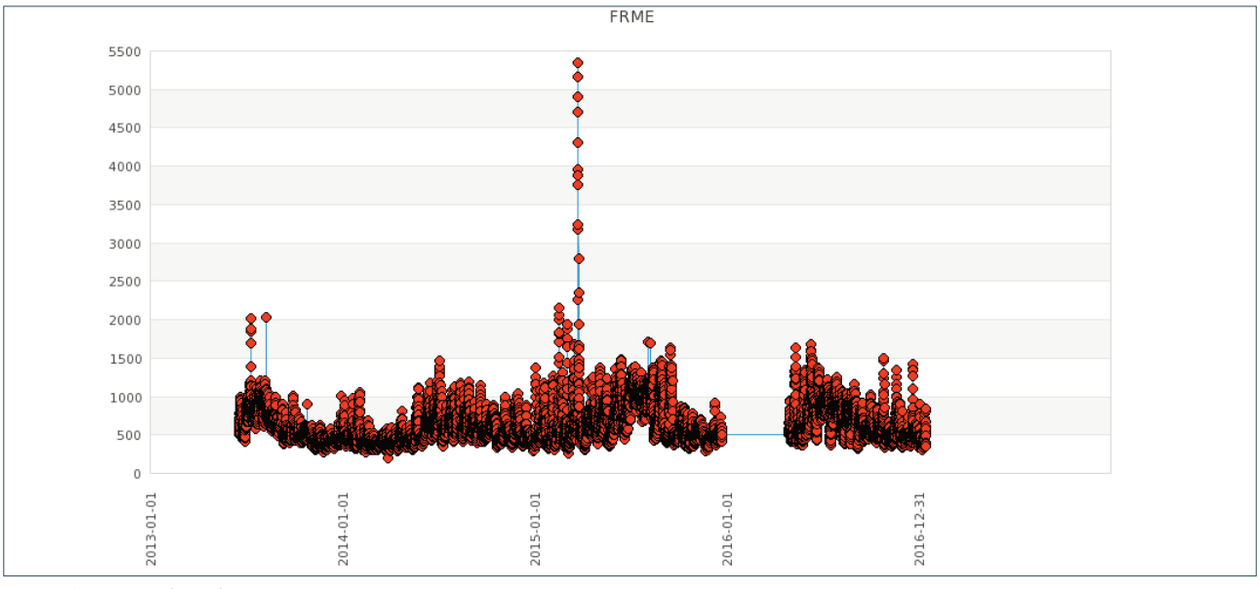

FIGURE S7. Radon (CPM) soil time-series from FRME station, as of November 2017.

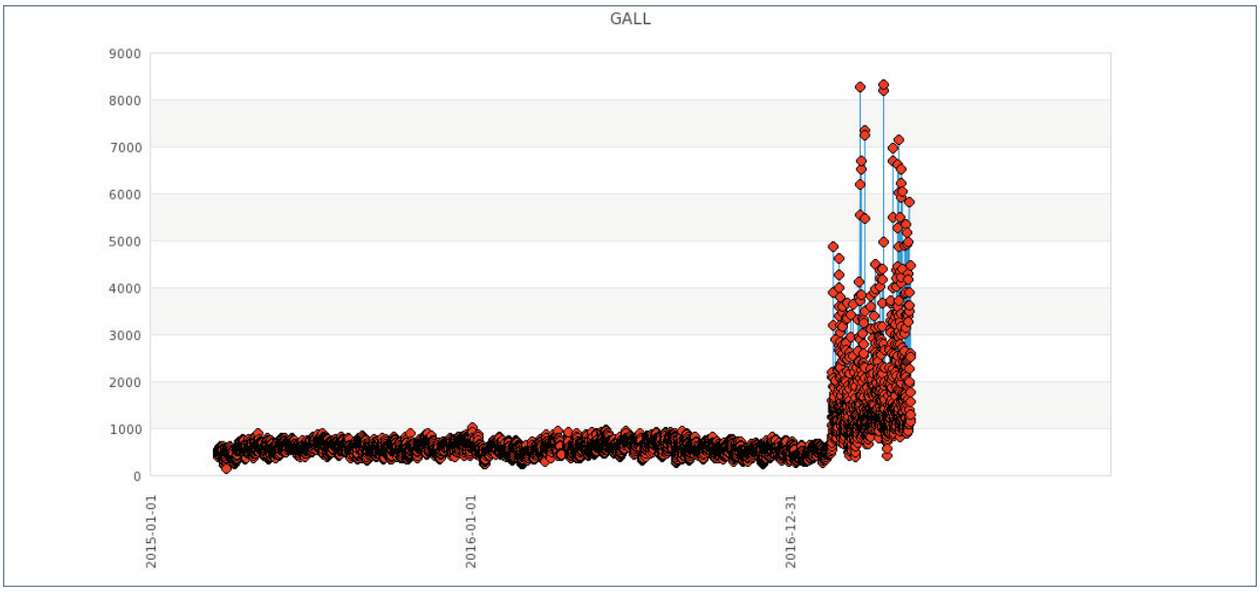

FIGURE S8. Radon (CPM) soil time-series from GALL station, as of November 2017.

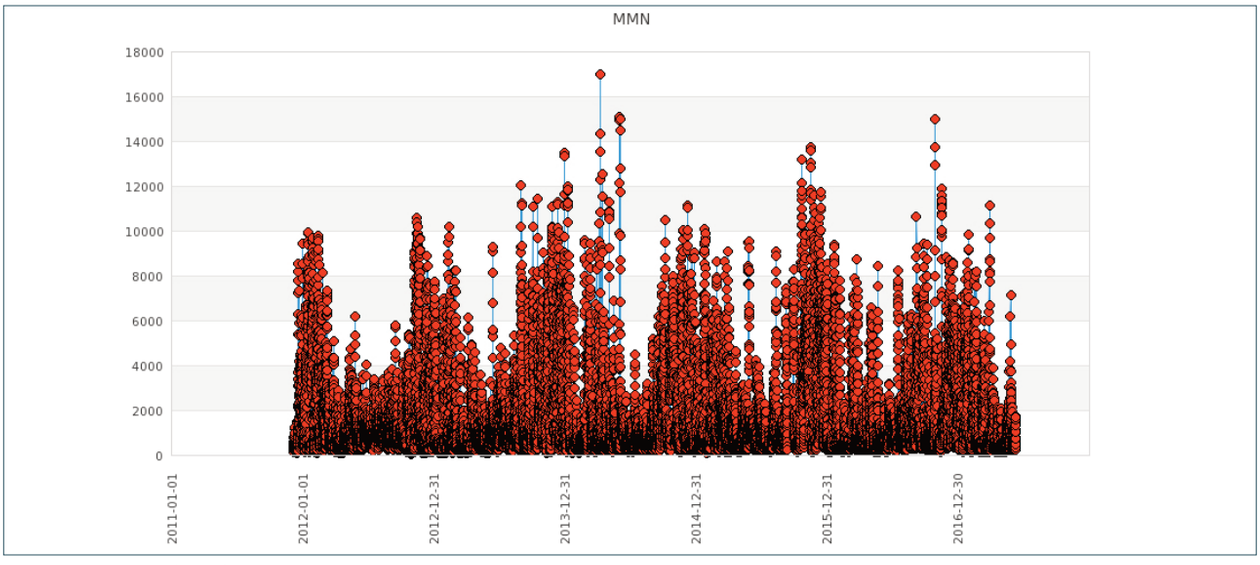

FIGURE S9. Radon (CPM) soil time-series from MMN station, as of November 2017.

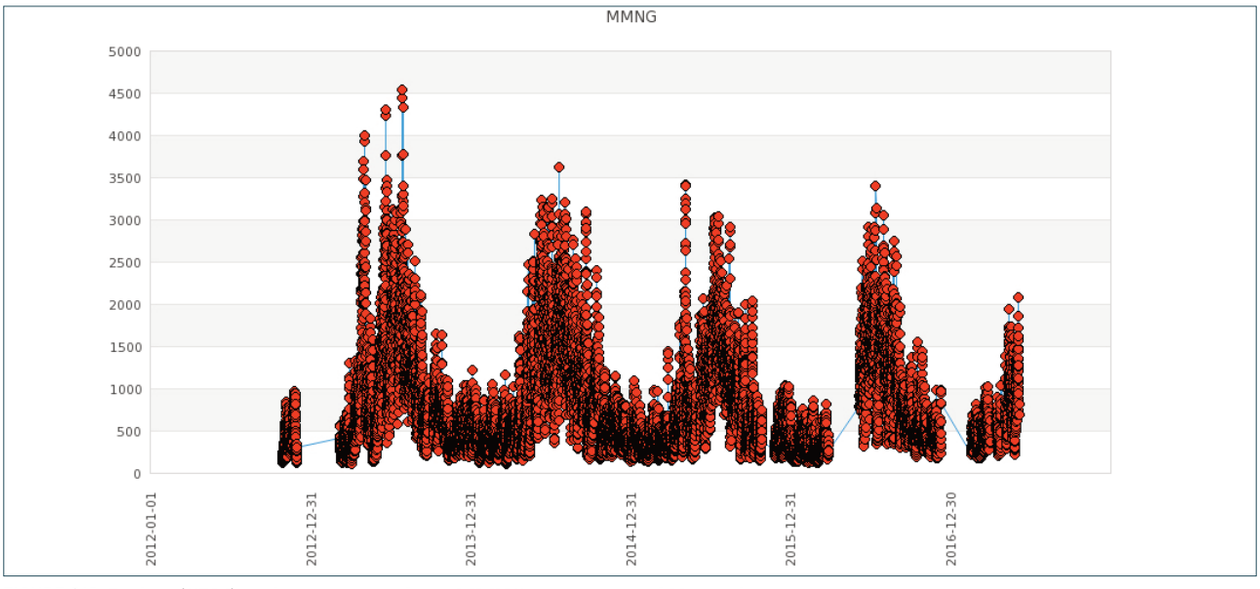

FIGURE S10. Radon (CPM) soil time-series from MMNG station, as of November 2017.

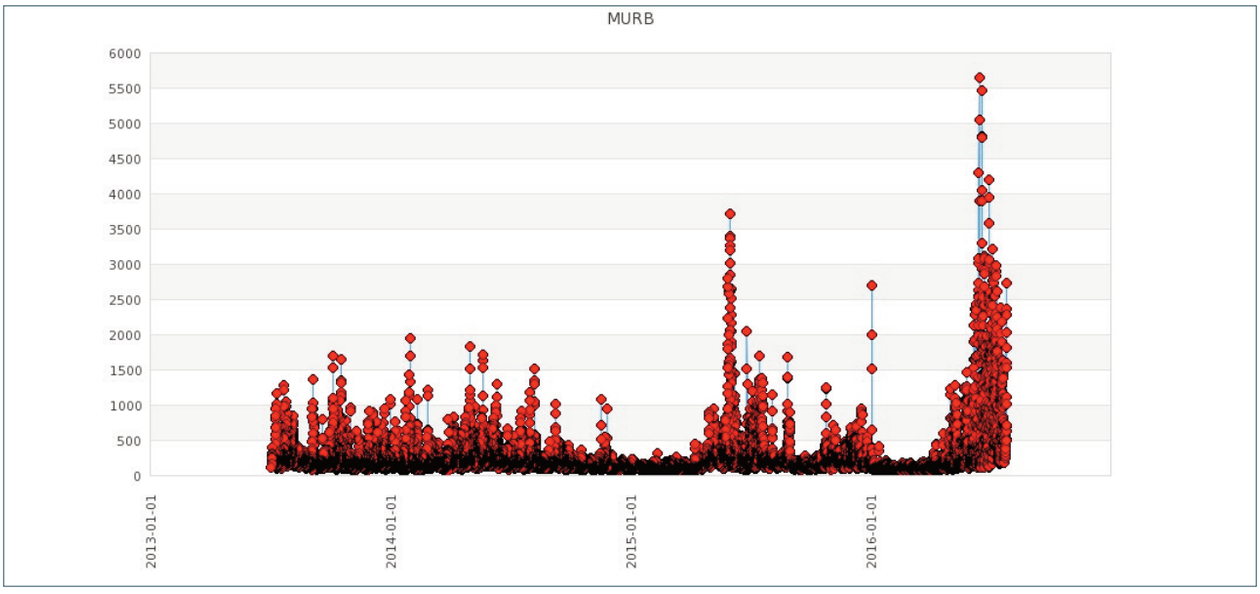

FIGURE S11. Radon (CPM) soil time-series from MURB station, as of November 2017.

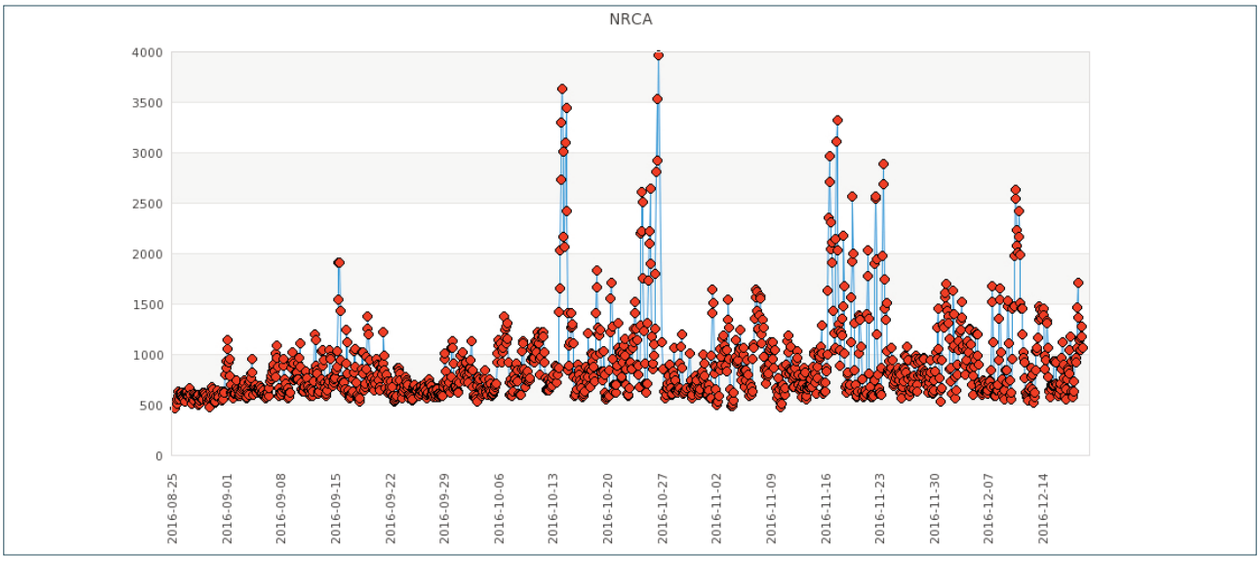

FIGURE S12. Radon (CPM) soil time-series from NRCA station, as of November 2017.

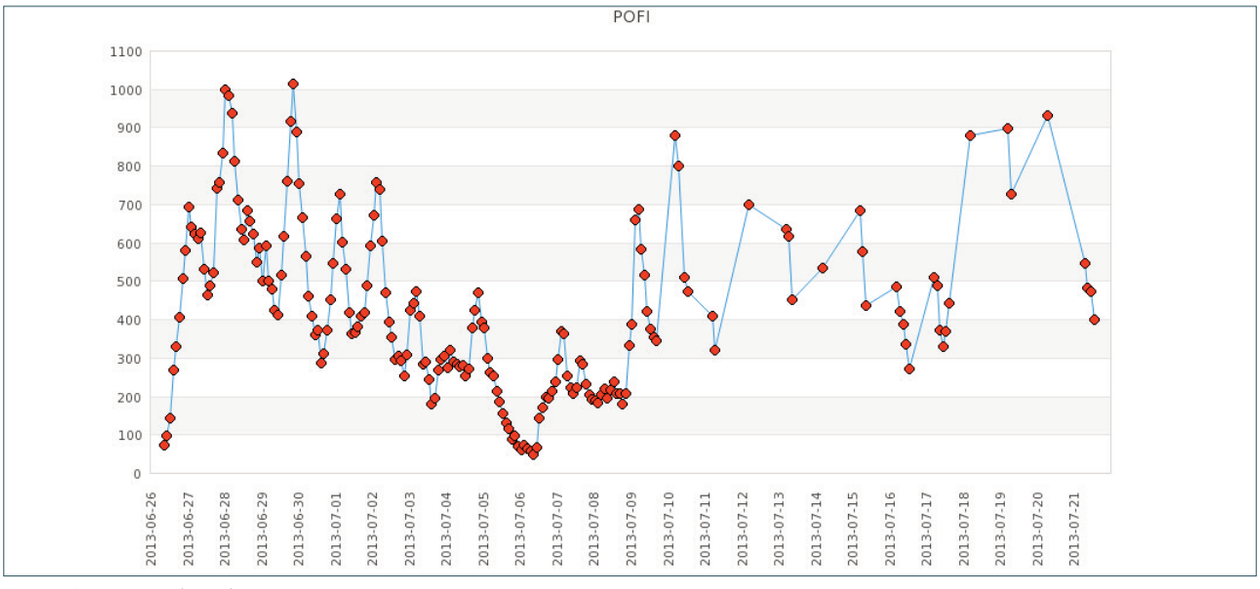

FIGURE S13. Radon (CPM) soil time-series from POFI station, as of November 2017.

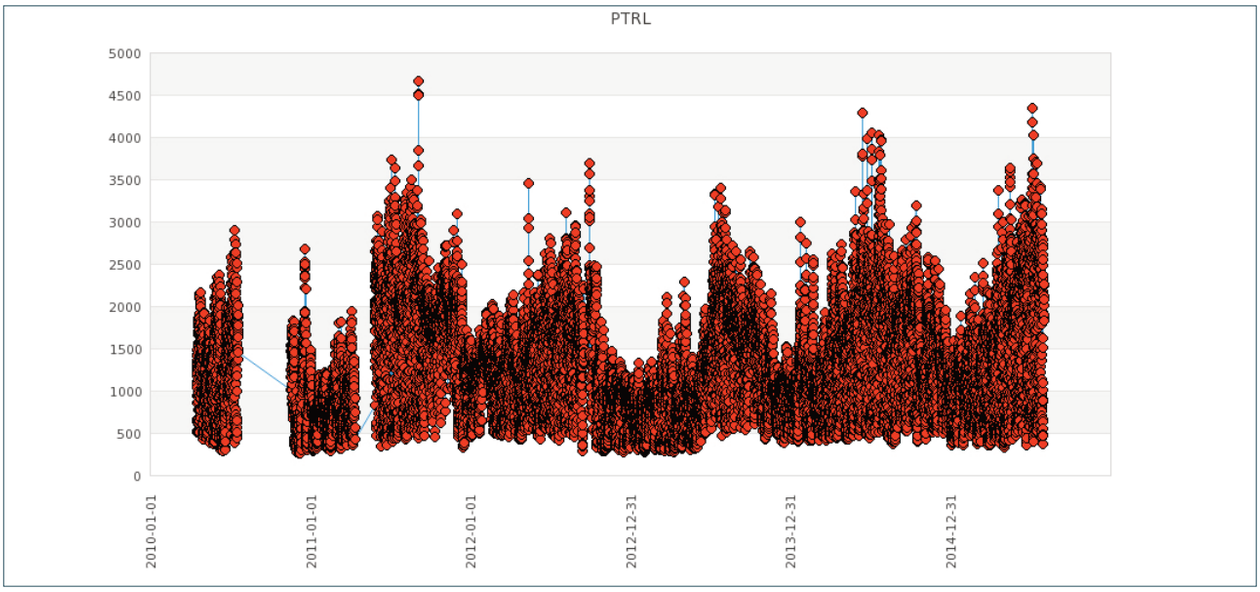

FIGURE S14. Radon (CPM) soil time-series from PTRL station, as of November 2017.

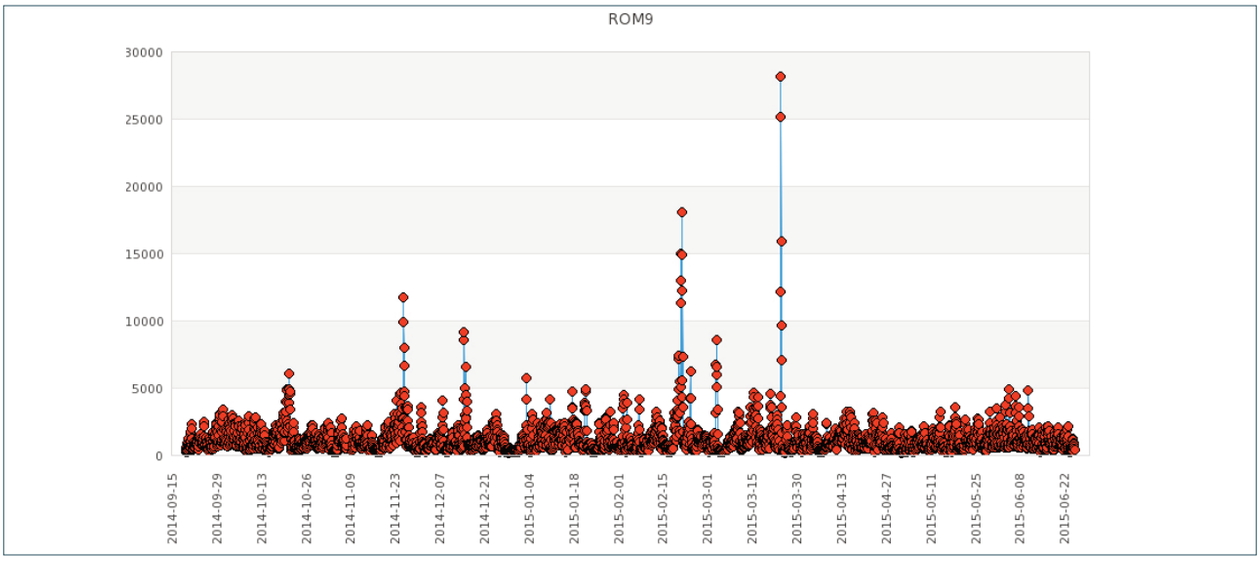

FIGURE S15. Radon (CPM) soil time-series from ROM9 station, as of November 2017.

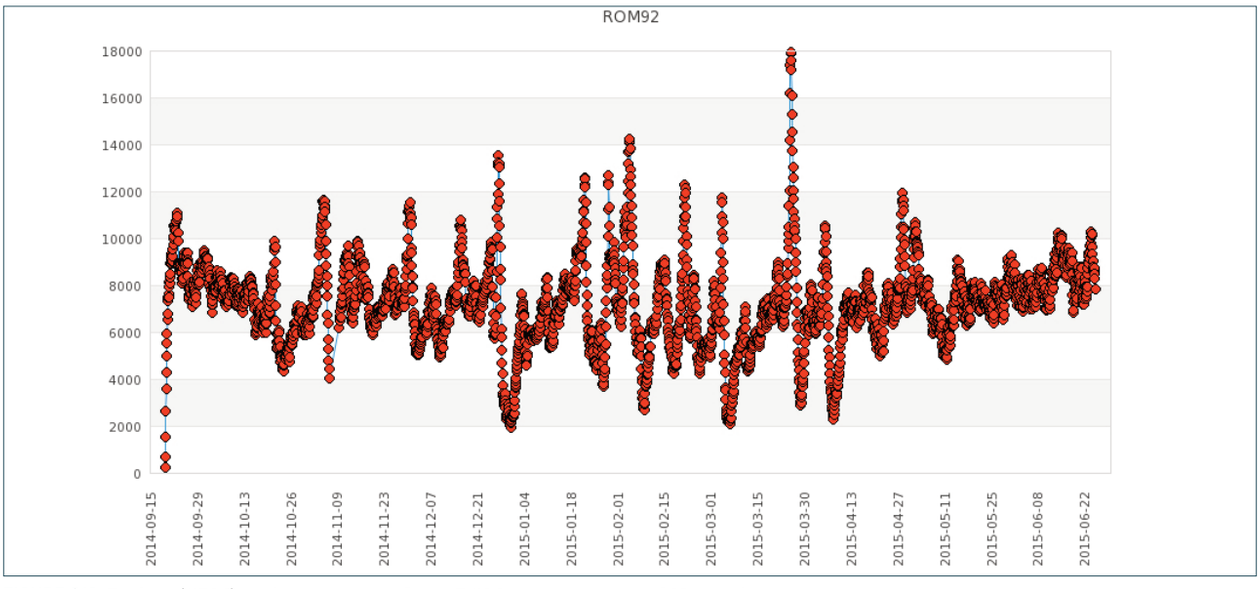

FIGURE S16. Radon (CPM) soil time-series from ROM92 station, as of November 2017.

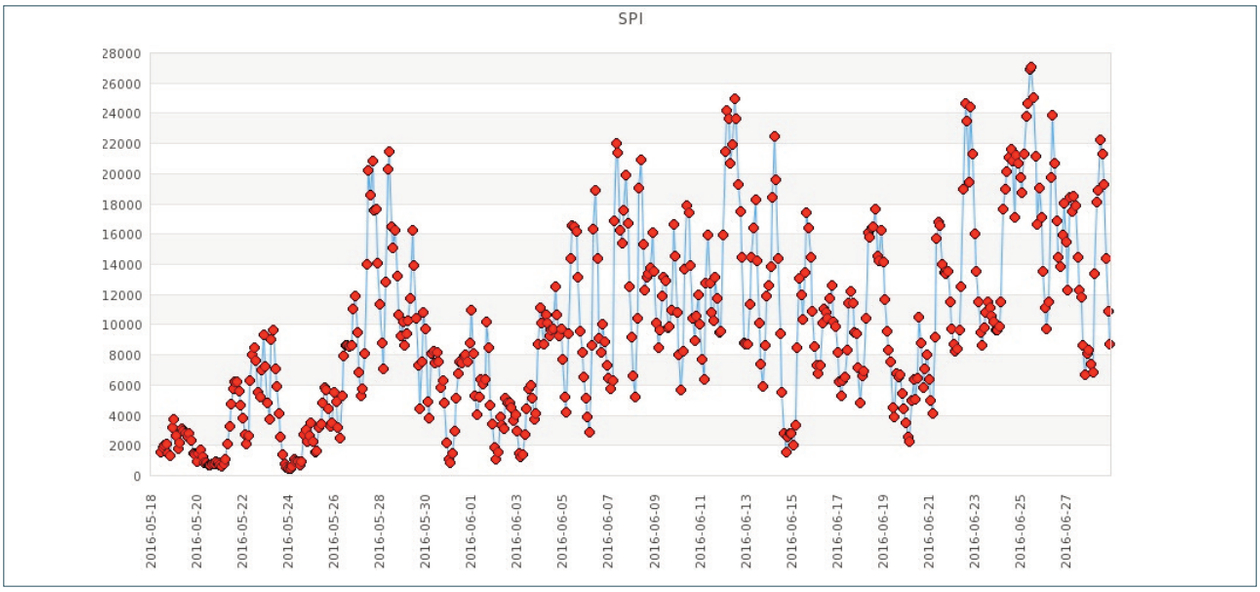

FIGURE S17. Radon (CPM) soil time-series from SPI station, as of November 2017.

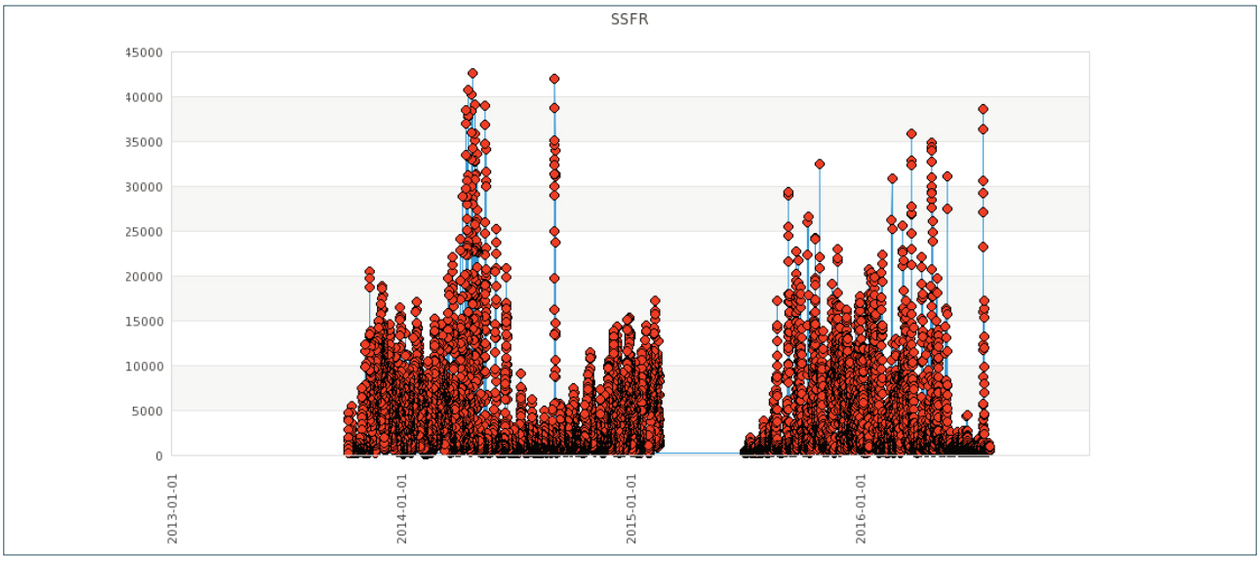

FIGURE S18. Radon (CPM) soil time-series from SSFR station, as of November 2017.